DD

**CHOOZ note 95/01**
**INFN PI/AE 95/06**
August 18th 1995



# The photomultiplier test facility for the reactor neutrino oscillation experiment CHOOZ and the measurements of 250 8" EMI 9356KA B53 photomultipliers



A. Baldini [a] C. Bemporad [a] E. Caffau [c] F. Cei [b] P. Cristaudo [c]
G. Giannini [c] M. Grassi [a] D. Nicolò [b] S. Parlati [a] R. Pazzi [a]
G. Pieri [a] S. Stalio [a] Y.M. Zhang [c]

[a] *INFN and Dipartimento di Fisica dell' Università, Pisa*
[b] *INFN and Scuola Normale Superiore, Pisa*
[c] *INFN and Dipartimento di Fisica dell' Università, Trieste*

**Abstract**

We describe a LabView controlled PMT test facility developed for the CHOOZ neutrino oscillation experiment. The results relative to the measurements of 250 8"-diameter $EMI\ 9356KAB53$ photomultipliers are presented.

*Submitted to Nuclear Instruments and Methods in Physics Research*

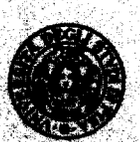

UNIVERSITÀ DEGLI STUDI DI PISA
DIPARTIMENTO DI FISICA

Istituto Nazionale di Fisica Nucleare
Sezione di Pisa

# The photomultiplier test facility for the reactor neutrino oscillation experiment CHOOZ and the measurements of 250 8" EMI 9356KA B53 photomultipliers

A. Baldini [a] C. Bemporad [a] E. Caffau [c] F. Cei [b] P. Cristaudo [c]
G. Giannini [c] M. Grassi [a] D. Nicolò [b] S. Parlati [a] R. Pazzi [a]
G. Pieri [a] S. Stalio [a] Y.M. Zhang [c]

[a] *INFN and Dipartimento di Fisica dell' Università, Pisa*

[b] *INFN and Scuola Normale Superiore, Pisa*

[c] *INFN and Dipartimento di Fisica dell' Università, Trieste*

**Abstract**

We describe a LabView controlled PMT test facility developed for the CHOOZ neutrino oscillation experiment. The results relative to the measurements of 250 8"-diameter *EMI* 9356*KAB*53 photomultipliers are presented.

*Preprint submitted to Elsevier Science*

## Contents

## 1 Introduction

The CHOOZ experiment is a long baseline search for neutrino vacuum oscillations at the homonymous nuclear power station [1]; the apparatus is conceived as a liquid scintillator low-energy, high-resolution "calorimeter" observed by 250 8"-diameter photomultipliers (PMTs). Neutrino events generate light which tipically activates 1/2 of the PMTs at a level corresponding to a few photoelectrons (*phes*) at each photocathode. The test facility was designed to determine relevant parameters in view of the optimized use of the PMTs in the experiment. Several measurements, performed on all PMTs, are listed:

(i) the operating high voltage (HV) corresponding to a 30 $mV$ pulse (on 50 $\Omega$) for a single photoelectron; this is what is needed to match the experiment electronics (discriminators, waveform digitizers, etc.);
(ii) the PMT noise level;
(iii) the relative light sensitivity (proportional to the photocathode quantum efficiency $\times$ the photoelectron collection efficiency);
(iv) the single *phe* pulse height spectrum and its peak to valley $(P/V)$ ratio;
(v) the PMT time characteristics; the transit-time at the operating high voltage, the transit time spread at the 1-*phe* level.

All these parameters were compared with the ones (or similar ones) contained in the PMT test ticket given by the producer. The data were also used to decide a proper geometrical arrangement of the PMT within the detector. We also digitized and registered, by a fast digital scope, a large sample of PMT pulses corresponding to 1-*phe* and to many *phe*'s. In addition to the main measurements, some other issues are under study on part of the PMTs:

(i) the PMT linearity of response with different HV dividers and with the divider finally selected;
(ii) the magnetic field effects on the PMT response;
(iii) the PMT prepulsing and afterpulsing at various light levels;
(iv) the noise time-dependence, after the PMT exposure to light;
(v) the signal cross talk among close PMTs.

The results will be presented in a separate paper.

We would like to stress that the development of a good and versatile, computer controlled, PMT test facility demands a considerable investment of time and effort; after its initial use for the CHOOZ experiment, it will be used, as a Pisa INFN laboratory facility, for other experiments under preparation or being planned. Several PMT test facilities were developed in the past; we mention the ones of the IMB [2] and of the Borexino [3] experiments.

## 2 The photomultiplier and the divider

The PMT type was selected according to the following requirements: large photocathode surface, high amplification, good (but not ultra-fast) time properties, good $P/V$ ratio in the single photoelectron pulse spectrum, low sensitivity to magnetic fields, low radioactive background, acceptable cost. The choice was a variety ($EMI\ 9356KAB53$) of the $EMI$ 9350 8"-diameter 14-dynodes photomultiplier. The high amplification ($\approx 10^7$) satisfies the electronics needs ($\approx 30\ mV$ for a single photoelectron pulse); the transit-time jitter ($\approx 8\ ns\ fwhm$ at the 1-*phe* light level) matches the liquid scintillator decay time ($\approx 7\ ns$); the B53 specification refers to the low radioactivity glass of the PMT envelope (Ultra Low Background glass: $K = 60\ ppm$, $Th = 20\ ppb$ $U = 10\ ppb$ [4]).
The voltage divider design and construction were optimized in order to comply with the stringent requirements imposed by the experiment on electrical, mechanical, chemical and radiopurity characteristics. The selected solution of surface mounting on printed circuit board (PCB) technique minimizes at the same time the electrical connections length, the total mass of the voltage divider base and thus the integrated mass of the small fraction of residual radioactive contaminants. At the last stages of the divider chain the charge storage capacitors are also of the surface mounting type while only two standard type, larger size, high voltage capacitors are required for the anode signal extractions and for the ground referencing of the charge storage system on the last dynodes. For what concerns the electrical characteristics of the voltage divider, instead of the "linear bleeder" version, with equal interdynode voltages, which maximizes the amplification for a given high voltage, we chose a "tapered bleeder" progressive divider type, with interdynode voltages progressively increasing in the last dynode stages. This solution, corresponding to the "O" option on the EMI data sheets, has been proved to provide enhanced linearity at a still acceptable high voltage for the required gain.
The PCB, with all components soldered on it, is a circular disk with a diameter equal to the one of the PMT socket so it is soldered to its pins and glued to the back of the socket itself. Around both a plexiglass cylinder encloses everything preventing contact of liquid scintillator with any other material except plexiglass and socket. Both high voltage and signal are carried by a single high quality teflon RG303, coaxial, 50 Ohm cable coming out of a sealed hole in the plexiglass cylinder. The divider layout is shown in fig.1.

## 3 The dark room and the mechanical structure

The test facility PMT holding structure, the light sources and the optical bench are all located in a dark room adjacent to the laboratory where the

control and data recording electronics and the computer are installed. The dark room is air-conditioned and it is equipped with red filtered lights; all operations on the PMTs: cleaning, mounting, dismounting, are performed under red lights to minimize the time needed to reach stable dark noise conditions. HVs are remotely controlled from the laboratory. A safety switch automatically kills the HVs, if they were not properly turned-off, when entering the dark room. A schematic drawing of the PVC and aluminum mechanical structure is presented in fig.2. It is light-tight and made of two separable sections: the cylindrical base holds the PMTs, the pyramidal top holds the light source at a distance of $\approx 188\ cm$ from the photocathodes. A maximum of 16 PMTs can be arranged along two concentric rings on a supporting plane. The internal and the external PMT rings subtend half-angles of 9.1° and 14.0° at the light source. Two Helmholtz coils are wound around the holding structure with a relative spacing optimized to generate a magnetic field, coaxial with the PMT axes, and as uniform as possible. The simmetry axis of the mechanical structure can be oriented in the earth magnetic field direction, which then becomes also the one of the PMT axes. The absolute value of the magnetic field in the dark room was measured by a rotating coil magnetometer; the field was also mapped, at the location of the device, by a three dimensional high sensitivity Hall-probe. Since the dark room is in an iron-reinforced concrete building, the magnetic field has rather large spatial variations over the volume occupied by the PMTs; it is then impossible to completely cancel the magnetic field by the Helmholtz coils and the apparatus orientation alone. We introduced therefore cylidrical mu-metal shields ($1\ mm$ thick, $25\ cm$ long), around the PMTs. The residual magnetic field at the photocathodes was then $< 20\ mG$ for the axial and $< 10\ mG$ for the radial field.

## 4 The optics

The light level of neutrino events in CHOOZ corresponds to a few initial *phes* at each photocathode; it is therefore this regime at which most of the PMT parameters must be determined. The best suited source is the Hamamatsu picosecond light pulser PLP-02 with a laser diode head SLD-041; this is a frequency- doubled diode emitting at $410\ nm$, a wavelength close to the maximum photocathode sensitivity. What makes this device particularly appealing is the short light pulse ($< 40\ ps$), the small time-jitter between the laser pretrigger and the light pulses ($< 10\ ps$), the small temperature dependence of the delay ($< 10\ ps\ /°C$), the stable pulse to pulse light emission and temperature stability (relative variation $< 1\%$ and a shift $< 1\%\ /°C$). Shortcomings are the low maximum light level ($\leq 10\ phe$ at each PMT), which cannot be modified and which makes the optical alignement difficult, and the non optimal light beam geometry. The laser can be triggered and provides a time-reference pre-

trigger pulse which is delayable, but, in our case, is simultaneous with the light emission. The laser head is mounted on a standard optical bench together with the other optical elements. The laser beam, $\approx 3 \times 3\ mm^2$ in size, is attenuated by a linear variable neutral density filter (Oriel 28629), remotely driven, and it is fed into a glass fiber optic cable (Oriel 77527, $\phi = 3.2\ mm,\ L = 1829\ mm$) by a short focal lens; an optimization is made for the optimum fiber light transfer. The other fiber end is inserted into a diffusing beam probe with opal diffuser (Oriel 77656) and this is connected to the vertex of the pyramidal part of the mechanical structure. Other light sources can be coupled to the pyramid through independent port holes; this allows their comparison and intercalibrations.

## 5 The system control and the data acquisition

### *5.1 The HV power supply, the NIM and CAMAC electronics*

The PMT HV and signal cable reaches the electronics racks, passing through light-tight apertures in the dark room wall; these cables are $RG303$ 11 $m$ long. The HV system is the CAEN SY527 mainframe with 16-channels cards A734P, supplying a maximum of 3 $KV$ positive voltage to the PMTs; the system is CAMAC controlled via the CAENET card C117B. Most of the acquisition system is standard CAMAC; the computer interface is the CERN-type 392 and the NU-bus card A410 (both produced by Bergoz). The electronics includes two 16-channels discriminators Phillips 7106, one 32-channels scaler Phillips 7132H, two 16-channels TDC's Phillips 7186H, a timing module Kinetics System 3655-L1A, I/O registers, logic units, etc.. The system includes ancillary NIM electronics: linear fan-in/out circuits (Phillips 748 and Lecroy 428F), fast PMT amplifiers (Phillips 776), gate/delay generators (Phillips 794). The CAMAC is controlled by a MacIntosh QUADRA 650, with an upgraded memory of 20 $MB$, a 17" monitor and high resolution card, for easy symbolic programming, and a $270MB$, removable cartridge, hard disk for permanent data storage. The acquisition system also includes a Tektronix TDS620 fast digital scope, GPIB interfaced, used for PMT waveform acquisitions. A simplified electronics layout is presented in fig.3; the different performed functions are detailed when discussing the measurement procedures.

### *5.2 The software*

The software is based on LabView 3.1 [5] integrated by the CAMAC control and histogramming routines developed at CERN [6]; this type of graphical

programming is indeed very powerful for applications like ours, since it can be easily adapted to rapidly evolving hardware configurations and it also offers good facilities for a first on-line data survey. Several instruments had no LabView drive available; we developed, in particular, new drivers for the CAEN HV power supply, and for the Newport precision movable tables.

## 6 The measurement program

### *6.1 The PMT database*

A database was prepared and filled with most of the information contained in the EMI supplied test tickets [1]. The relevant parameters are: the serial number, the luminous sensitivity, the dark current, the HV for a 3 $10^7$ gain, the $P/V$ ratio in the single photoelectron spectrum. After the test the database was updated with the measured parameters. Also recorded was the position of each PMT in the facility during the test. A PAW-ntuple was derived and updated from the database for conveniently processing, studying and plotting the results.

### *6.2 PMT installation and measurement of the dark-adaptation time*

The 16 PMTs were installed in the testing facility under red light. In the case of a non perfectly clean photocathode, its surface was cleaned with isopropyl alcohol. The PMT was always positioned with the dynode plane oriented in the East/West direction. The device was then closed, the compensating magnetic field was turned on, and the dark room was abandoned and sealed. HVs were switched on at 90% of the value given by EMI for a 3 $10^7$ gain and the PMT signals were observed on an oscilloscope for a first check of their regular behaviour. The PMTs were left with HV-on overnight for $\approx 12$ *hours*; during this time the dark noise was measured for $\approx 10$ $s$ at 15 $m$ intervals, and the information was directly stored into a file. The noise rate vs time curves for each PMT are then fitted by the combination of two exponential functions plus a constant; we obtain therefore the initial noise level, its (two decay constants) decrease, and the extrapolated, infinite time, level. One is then ready for the operating voltage determination. The noise level is later remeasured at the operating voltage.

[1] We refer to the 1993 EMI catalogue [4] for details on their parameter determinations

*6.3 The determination of the PMT operating voltages*

The CHOOZ experiment requires a PMT single photoelectron 30 $mV$ pulse on 50 $\Omega$ at the electronics hut; this means a PMT amplification of $\approx 1.5\ 10^7$. The search for the operating point is based on the determination of the PMT efficiency curve, at a fixed discriminator threshold of 30 $mV$, as a function of the HV; the laser light level was chosen to have a PMT efficiency of $\approx 22\%$ ($\geq 88\%$ pure single *phe* pulses), the laser repetition rate was 1 $KHz$. If the efficiency curve could be followed up to HVs corresponding to the plateau efficiency $\epsilon$, one would directly determine the HV corresponding to $\epsilon/2$ as the operating voltage; unfortunately this would bring most PMTs into a dangerous HV region. One can avoid problems by measuring, at the same time, the efficiency curves relative to a 30 $mV$ and to a 10 $mV$ threshold; this requires the use of two discriminator channels for each PMT; one of the PMT fan-out outputs is directly connected to the 30 $mV$ threshold discriminator, a second output is $\times 10$ amplified and is connected to a 100 $mV$ threshold discriminator. One can measure $\epsilon$ and $\epsilon/2$ by the amplified channel curve (the equivalent threshold is 10 $mV$) and one can determine the HV corresponding to $\epsilon/2$ on the 30 $mV$ curve. This double-curve method is fast and effective; it was previously used for the IMB experiment [2]. The real measurements are performed according to a much more complex pattern to protect the PMTs from any damage. The PMT HVs are initially set at $-350$ $V$ under the 90% of the HV value given by EMI as corresponding to a gain of $3\ 10^7$; with the laser light off, one measures the noise curves as a function of the HV, in 50 $V$ steps and by 2 $s$ counting time intervals; when a background level of 5 $KHz$ is reached, the HV is recorded and the corresponding PMT is switched off; this program goes on, testing the noise of all other PMTs up a maximum voltage of 2000 $V$. The cycle then restarts from the initial HVs; one measures again the noise level with laser off, then one measures, with laser on, the PMT efficiencies (by $2\ 10^4$ laser pulses in 20 $s$); the HVs are increased by 50 $V$ and a new measurement begins; this goes on up to 2000 $V$ while all PMTs which reached an excessive noise level are automatically switched-off; a data file is constantly updated. At the end of these measurements the 32 normal and amplified channel curves are displayed on the MacIntosh screen. The operating HV can be directly extracted from the display, but, for a better uniformity in the procedure, we preferred to derive the operating voltage from an off-line fit to the curves from the data file. Note that the curves always show plateaux which are not horizontal (see fig.5); this is due to the extremely variable single photoelectron pulse shape and to the use of normal (non constant fraction) discriminators. All the procedure can be compared and checked by ADC PMT spectra (see § 6.4) taken at the operating voltage; although ADCs provide a pulse charge measurement and depend therefore on the particular PMT pulse shape, the relation between pulse height and pulse time-integral appears to be independent of the particular PMT. It is worth noting that a determination

of the operating voltage based on the use of the ADC spectra alone would be much more time consuming than the method based on the use of scalers and on the measurement of the efficiency curves, since ADCs and this CAMAC system have a maximum data taking rate of $\approx 100\ Hz$.

### *6.4 The single photoelectron spectrum and the time characteristics*

The single photoelectron spectrum, the transit time and the transit time spread were measured, 16 PMTs at a time, at the PMT operating voltages; the transit time variation as a function of the HV was also measured for several PMTs. The data collection for these measurements is controlled by a separate program; the laser is fired at a 100 $Hz$ rate; data files and histograms are updated every 500 laser pulses; a typical run collects $\approx 3\ 10^4$ laser pulses. The ADC gate is 250 $ns$, the TDC common stop is given after 300 $ns$; pedestals are registered at the end of each measurement, with the laser light emission switched-off. At the end of run, the 16 ADC spectra and the 16 TDC spectra are displayed on the MacIntosh screen. The data analysis is performed off-line on the data files.

### *6.5 The determination of the PMT relative sensitivity*

The PMTs will be positioned in the apparatus so as to reach a uniform sensitivity to the event light; one must therefore know the PMT relative sensitivities [2] ; since the chosen operating voltages provide the same photoelectron pulse heights, the relative sensitivity really means something proportional to the product of the PMT quantum efficiency ($QE$) and of its collection efficiency ($CE$). All measurements performed on the various 16-PMT groups by the Hamamatsu laser were also referred to two other "passive light sources": 1) a disk of $NE110$ fast scintillator ($\phi = 5\ cm\ t = 1\ cm$) activated by a low intensity (30 $KBq$) $^{60}Co$ $\gamma$-source; b) a $^{241}Am$ $\alpha$-source on a $NaI$ crystal (a Harshaw "pulser"). While the $NaI$ light is diffused by an opal glass diffuser, the $NE110$ light source has only a white paper diffuser on the back of the scintillator disk.

Such comparisons among different light emitters were considered necessary because, a priori, the use of "passive light sources" guarantees a better reference than the laser and fiber optics PMT illumination; this depends on the long term laser stability, on the optical bench alignment, on the fiber optics position (the mounting and dismounting of PMTs requires the fiber optics detachment before opening the test facility). The three light sources emit light with slightly different angular distributions; the corresponding differences at

[2] we did not measure the PMT absolute sensitivities

the two PMT concentric rings must be corrected for by appropriate factors; the ratio of the light intensity between the inner and outer ring was determined by interchanging, several times, groups of PMTs of the two rings. The correction factors between inner and outer ring is $1.16 \pm 0.04$ for the laser and the $NE110 + {}^{60}Co$ source and $1.23 \pm 0.08$ for the $Am + NaI$ source, both much larger than the ones due the Lambert's cosine law alone.

### *6.5.1 Relative sensitivity by the Hamamatsu laser*

The laser was operated at a low light intensity corresponding $\approx 0.25$ *phes* at each PMT, the laser repetition rate was 100 $Hz$. The pedestal and the *phe*-distributions (1-*phe* dominated) are fitted by a gaussian function and by the sum of the poissonian terms for $1-$, $2-$, $3-$ ... *phes* (see fig.10); each of these terms is represented by a gaussian function whose peak position and width are given by: $p_n = np_1$ and $\sigma_n = \sigma_1\sqrt{n}$ [7,8]. The fit determines the fraction of events contained in the pedestal, i.e.: the Poisson probability $P(0) = e^{-\mu}$, where $\mu$ is the average number of *phes* measured by a particular PMT; $\mu$ represents therefore the PMT relative sensitivity.

### *6.5.2 Relative sensitivity by the $NE110 + {}^{60}Co$ light source*

The scintillator emits a low light intensity (correponding to an average of $\approx 0.9$ *phes* at each PMT), spectrally well matched to the photocathode sensitivity. While the laser has a pulse-to-pulse, stable light emission, the scintillator emits light whose variable intensity depends on the amount of the Compton recoil electron energy lost in the scintillator; the previous expression $P(0) = e^{-\mu}$ should then be averaged over the (stable) light intensity distribution. The intensity distribution was computed, by the Montecarlo method, for the geometry of our $NE110 + {}^{60}Co$ source and the average of $P(0)$ (and of all $P(n)$) was evaluated numerically. A flat intensity distribution is a rough approximation to the true distribution; nevertheless, at the $\approx$ 1-*phe* level, the averages obtained by a flat distribution are close (within 1% for $\langle P(0)\rangle$, within 6% for $\langle P(3)\rangle$) to the ones obtained by the true distribution. We give therefore the analytic expressions corresponding to the flat distribution:

$$\langle P(0)\rangle = (1 - e^{-2\mu})/(2\mu) \; .$$

The average number of *phes*, $\mu$ corresponding to the measured value of $\langle P(0)\rangle$ is obtained by the numerical inversion of the previous expression; $\mu$ represents the PMT relative sensitivity. While, in the laser case, the ADC spectrum is fitted by the sum of poissonian terms, in the $NE110$ case these terms must

also be averaged over the flat light intensity distribution:

$$\langle P(n)\rangle = (\int_0^{2\mu} x^n e^{-x}\, dx)/(2\mu n!)$$

$$\langle P(n)\rangle = [1 - e^{-2\mu} \sum_{k=0}^{n} \frac{(2\mu)^k}{k!}]/(2\mu),$$

where $n$ is the number of *phes* and noting that, for a flat distribution, if $\langle n\rangle = \mu$, the maximum number of *phes* is $n^{max} = 2\mu$.
When using a radioactive source, one must find a way to generate an ADC gate in coincidence with the light emission; this problems does not exist for the Hamamatsu laser which provides its own pretrigger pulse. The gate is present, in our case, each time a majority $M \geq 2$ within 50 $ns$ is generated by the 16-channels PMT discriminator; this majority condition is always ($> 99.9\%$) reached in the case of the $NE110$ light emission, while its occurrence is negligible in the case of the uncorrelated PMT noise. It is interesting to note that a majority request represents a potential bias in the sensitivity determination, since it corresponds to a minimum threshold for the light emission intensity; this is not a problem in our case: the majority $M \geq 2$ condition is always reached and we only measure relative sensitivities which are unaffected by a small global variation of the light intensity at all PMTs.

### *6.5.3 Relative sensitivity by the $NaI + ^{241}Am$ light source*

This light source has diameter and thickness $\Phi = 7\ mm\ t = 7\ mm$; it provides $\approx 10^3$ *pps* with a pulse-to-pulse stable light intensity. When permanently mounted behind an opal diffuser and close to the laser fiber optics at the top of the pyramid, it gives light pulses corresponding to $\approx 14$ *phes* at each PMT. The pulser light is emitted with a spectrum reasonably well matched to the photocathode sensitivity and with the typical emission time of $NaI$ detectors ($\approx 200\ ns$); the light can be switched-on and -off by a mechanical shutter. The data corresponding to the $Am + NaI$ source are collected with a 1.5 $\mu s$ ADC gate; the gate is present when a majority $M \geq 2$ is generated. Measurements with the $NaI + ^{241}Am$ light source are potentially more precise because of the high light intensity, but the use of this source is somewhat inconvenient for grounded cathode PMTs: we had to modify the PMT base capacitive output stages to reach time constants of 1.5 $\mu s$ for these particular measurements. Note that the relative sensitivity is measured by the average number of *phes* at each PMT; this is directly obtained from the (multi-*phes*) ADC gaussian spectra: $\mu = (P/\sigma)^2(1 + a)$, where $P$ and $\sigma$ are the, pedestal subtracted, peak position and width of the gaussian spectrum and $a$ is a $\approx 20\%$ correction taking into account the position and intrinsic width of the 1-*phe* spectrum [7]. The

method differs from the previous ones, since it depends on the measurement of pulse areas and not only on pulse counting.

## 7 Analysis and results

### *7.1 Dark adaptation time, operating voltage, dark noise rate*

The variation of the PMT noise during the $\approx$ 12 $h$ of conditioning time is shown in fig.4 for 4 PMTs. The experimental points can be fitted by the combination of two exponential functions plus a constant; a single time-constant fit is not adequate; the parameters are different for different PMTs.
The efficiency curves for 4 PMTs, corresponding to the two thresholds of 30 and 10 $mV$, are shown in fig.5 together with their fits; the fitting 5-parameter function is the sum of a straight line and of the integral $(erf(x))$ of a gaussian function. The operating voltages, obtained by the method discussed at §6.3, are distributed according to the histogram of fig.6. Successive repeated measurements reproduce the operating voltages within a $\sigma_V \approx 15\ V$ ; at the typical operating voltage the relation between the variation of the PMT gain and a HV variation is $\Delta G/G \approx 10 \times \Delta V/V$.
The results of our measurements are plotted in fig.7 against the corresponding HV values given by EMI for an amplification of 3 $10^7$; the correlation of the two determinations is extremely good.
The dark noise rates, measured at a 30 $mV$ threshold and at the operating voltage, after $\approx$ 12 $h$ from HV turn-on [3], are distributed according to the histogram presented in fig.8; although the dark noise rate can have large variations if remeasured after some days or after time-spaced HV switching-on and -off, the correlation with the dark noise, measured by EMI, under different conditions, is very poor (see fig.9).

### *7.2 The 1-phe spectrum*

All measurements were performed at the PMT operating voltage. The ADC and TDC spectra were simultaneously registered, at the 1-*phe* laser light level. The ADC spectra for 6 PMTs are presented in fig.10; the 1-*phe* peaks are well separated from the pedestal; the *phe* distributions are well fitted by the model of §6.5.1; the fits and their $1-$, $2-$, $3-\ldots$ *phes* components are also shown in fig.10. The distribution of the (pedestal subtracted) peak positions is shown in fig.11 for all PMTs; $\approx 1/2$ of the width of this distribution is due to

[3] for PMTs always handled under red light

small differences in the PMT gain (30 $mV/phe$) due to the operating voltage associated error ($\sigma_V/V \approx 1\%$, therefore $\sigma_G/G \approx 10\%$); this is an indication that the relation between pulse height and pulse charge is, within $\approx 10\%$, the same for all PMTs. The peak-to-valley ratio P/V, a parameter frequently used as an estimate of the width of the 1-*phe* spectrum, can be unambiguously determined from the fits of fig.10; the P/V distribution is presented in fig.12; our determination of the P/V ratio is compared, in fig.13, with the one given by EMI.

### *7.3 The relative sensitivity*

In addition to the ADC spectra obtained by the Hamamatsu laser and shown in fig.10, we present, in fig.14, 4 ADC spectra by the $NE110 + ^{60}Co$ and 4 by the $NaI + ^{241}Am$ light pulsers; the fits to the $NE110$ data, obtained according to the model at §6.5.2, are also shown.
The independent determination of the PMT sensitivities was derived from the Hamamatsu laser, the $NE110 + ^{60}Co$ and the $NaI + ^{241}Am$ data, according to the procedure introduced at §6.5; the $NaI$ method was only applied to a small PMT sample. The PMT relative sensitivity distributions are presented in fig.15a (laser) and fig.15b ($NE110$) together with their gaussian fits; they are very similar and narrow. The scatter plot of the $NE110$ results ($y$-coordinate) vs the laser results ($x$-coordinate) is shown in fig.16; the two sensitivity determinations are strongly correlated; if we renormalize the data to the same mean values $\langle x \rangle = 1$ , $\langle y \rangle = 1$ and we introduce an orthogonal reference system $\eta = y + x$ and $\xi = y - x$, the distribution of the data points is gaussian in the $\xi$ coordinate, with a $\sigma_\xi = \sqrt{{\sigma_x}^2 + {\sigma_y}^2} \approx 0.05$. One can therefore state that each of the two method has an accuracy better than 5% in the relative sensitivity determination. The scatter plot of the $NaI + ^{241}Am$ vs the $NE110 + ^{60}Co$ measurements, for 32 PMTs, is shown in fig.17. It is interesting to compare our sensitivity determinations ($QE \times CE$) with the $QEs$ declared by EMI ; the QE measured by EMI is a determination of the photocathode sensitivity alone (obtained, moreover, under conditions far from a normal PMT operation); the scatter plot of our $NE110$ vs EMI data is presented in fig.18.

### *7.4 The time characteristics*

The TDC time distributions for 6 PMTs, obtained at the 1-*phe* light level by the Hamamatsu laser, are presented in fig.19; all spectra show, in addition to the main peak, a small satellite at $\approx 65$ $ns$ after the first peak; the satellite signals are not real "aftepulses", but are only present when the normal pulse is absent.

The PMT transit time at the operating voltage is $\approx 100\ ns$. A scatter plot of the PMT relative transit time vs the operating voltage is presented in fig.20; the measured relative delays are useful if one wants to obtain a good PMT synchronization by cable length adjustment; the dependence of the transit time ($Tr$) on the HV, is $\Delta Tr/\Delta V \approx 0.03\ ns\ V^{-1}$. The histogram of the transit time fluctuations ($\sigma_{Tr}$) of all PMTs at their operating voltages is presented in fig.21; $\sigma_{Tr} = 3.8\ ns$, close to the value quoted by EMI.
The derivation of the corrections for the time-slewing introduced by the discriminators is important for any future analysis, in particular, for the determination of event positions. Since the electronics of the experiment will be quite similar to the one we used in the test facility, the correction is easily obtainable from "laser generated events" corresponding to simultaneous ADC and TDC measurements. Two scatter plots of the ADC-charge against the TDC-time, taken at two different light levels, are presented in fig.22a; the average times corresponding to each ADC charge slice are shown in fig.22b; these last distributions are well fitted by the function $a + b/\sqrt{Q}$ where $Q$ is the ADC measured charge.

### *7.5 Waveforms*

A collection of pulse waveforms, registered by the TDS620 digital scope at the 1-*phe* light level, is presented in fig.23; one can appreciate the large shape variations associated with such pulses. This type of data is relevant for a correct simulation of the Chooz experiment behaviour by the Montecarlo method.

### *7.6 PMT failures*

We had to discard 9 PMTs over the tested 250; they were sent back to EMI for inspection in view of their replacement; 5 units were hopeless: one arrived with cracked glass, the other four were discharging even at low voltages. 4 units had different problems: very high noise, very bad $P/V$ ratio, high level of afterpulses.

## 8 Conclusions

We measured several parameters, characterizing the PMT behaviour, on all the photomultipliers of the CHOOZ experiment. The test had a duration of $\approx 45\ days$ (several PMT groups were measured several times), while the start off and the complete debugging of the facility required $\approx 6\ months$. We intend

to complete the PMT measurements for CHOOZ by an improved investigation of the magnetic field effects, and of the prepulse and afterpulse frequency, amplitude, and time distribution; this study is already under way with our test facility on a PMT partial sample.

## Aknowledgments

We thank the colleagues of the CHOOZ collaboration for comments and discussions. We thank Yves Declais for the well timed help in providing the magnetic shield material. Very useful discussions are aknowledged with Giovanni Ranucci of the BOREXINO collaboration.
We wish to aknowledge the technical contributions by Giuseppe Fausto and Roberto Ruberti, of the Pisa INFN laboratory.

## References

[1] The CHOOZ collab., **The CHOOZ experiment**, Proposal June 1993 (available on WWW)

[2] C.R. Wuest et al., **Nucl.Instrum.&Meth. A239** 467 (1985)

[3] G. Ranucci et al., **Nucl.Instrum.&Meth. A337** 211 (1993)

[4] The Thorn EMI Inc. photomultipliers and accessories catalogue 1993

[5] LabVIEW is a trademark of the National Instruments Corporation, 6504 Bridge Point Parkway, Austin, TX 78730- 5039

[6] ©CERN, Geneva 1991

[7] E.H. Bellamy et al., **Nucl.Instrum.&Meth. A339** 468 (1994)

[8] G. Ranucci et al., **Nucl.Instrum.&Meth. A333** 553 (1993)

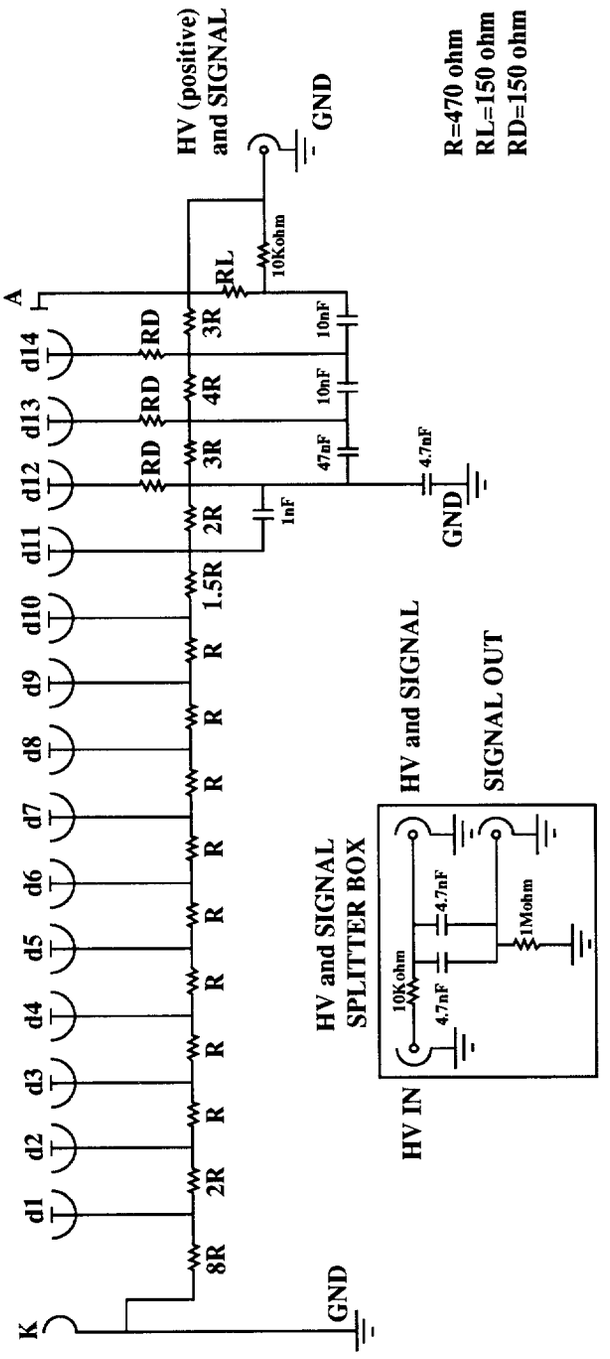


Fig. 1. The HV divider and the signal splitter box for the EMI $9356KA$ photomultiplier.

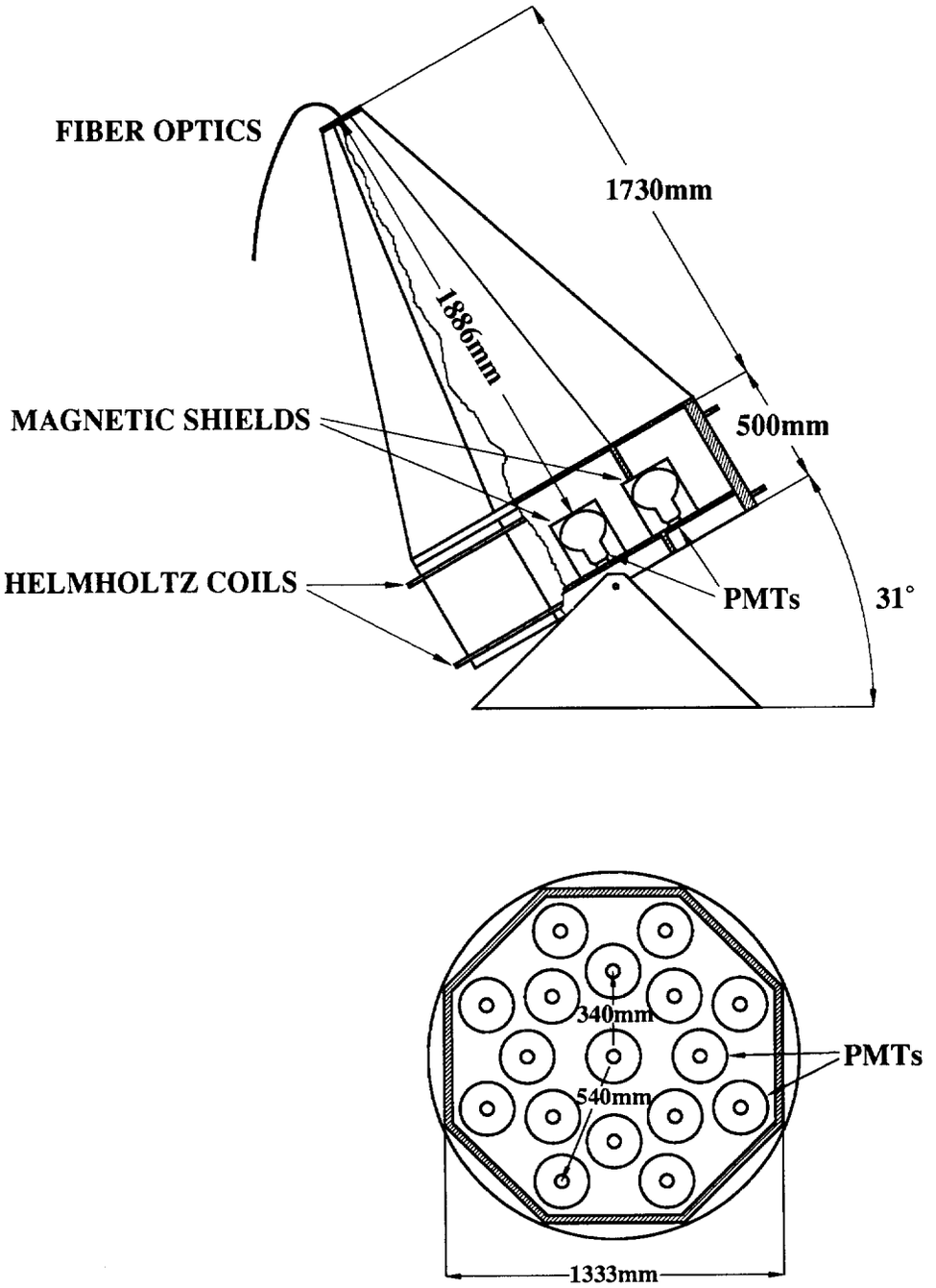


Fig. 2. Two views of the structure of the CHOOZ photomultiplier test facility.

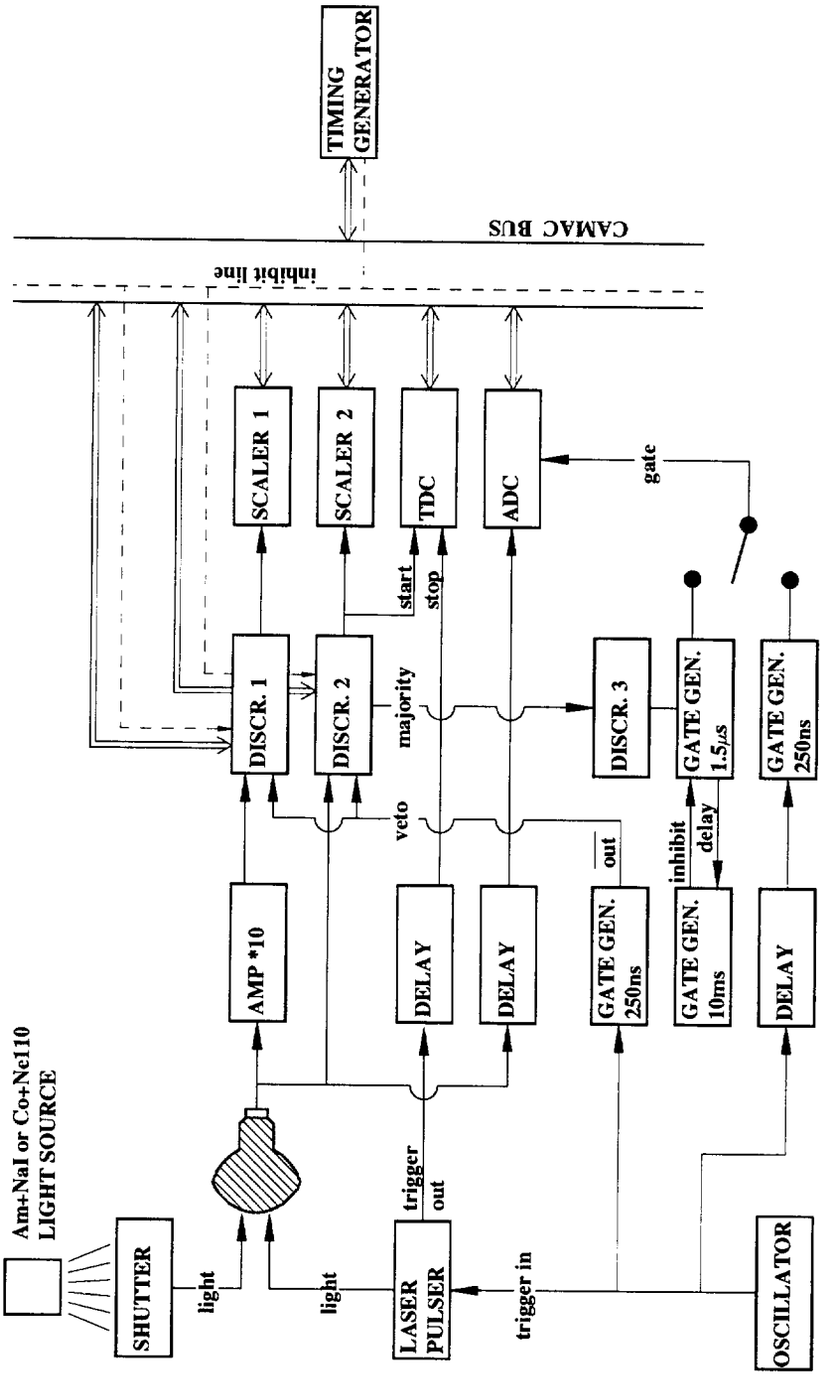


Fig. 3. The NIM and CAMAC trigger and data acquisition electronics.

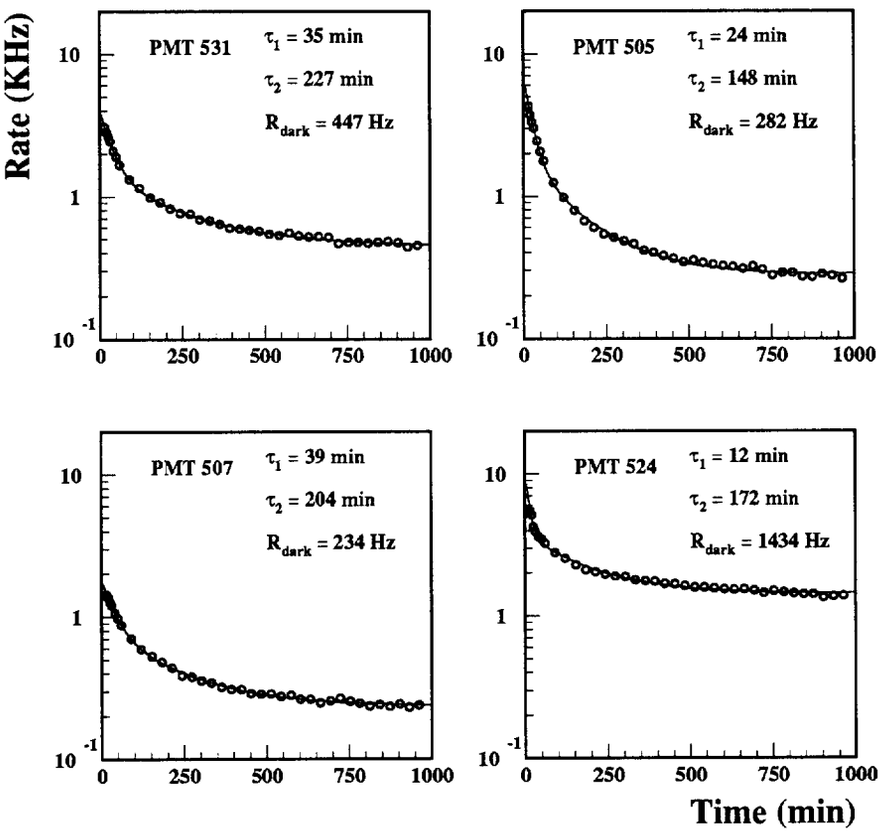


Fig. 4. The dark noise rate variation with time and a two exponential function fit.

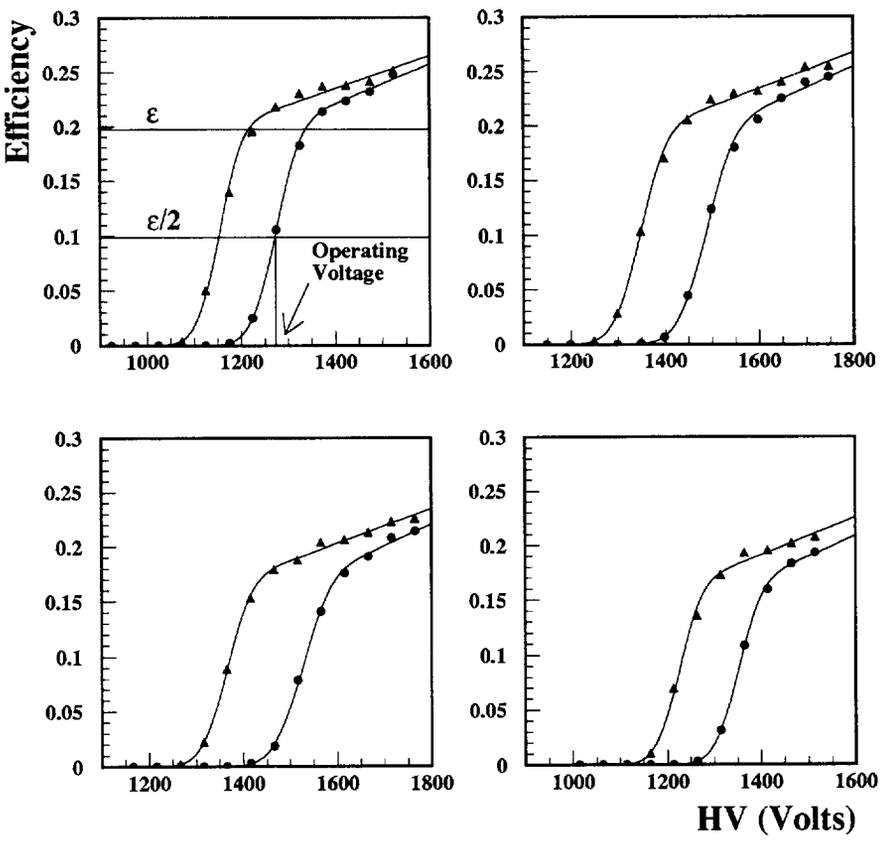


Fig. 5. Efficiency curves for 4 PMTs at 10 and at 30 $mV$ thresholds

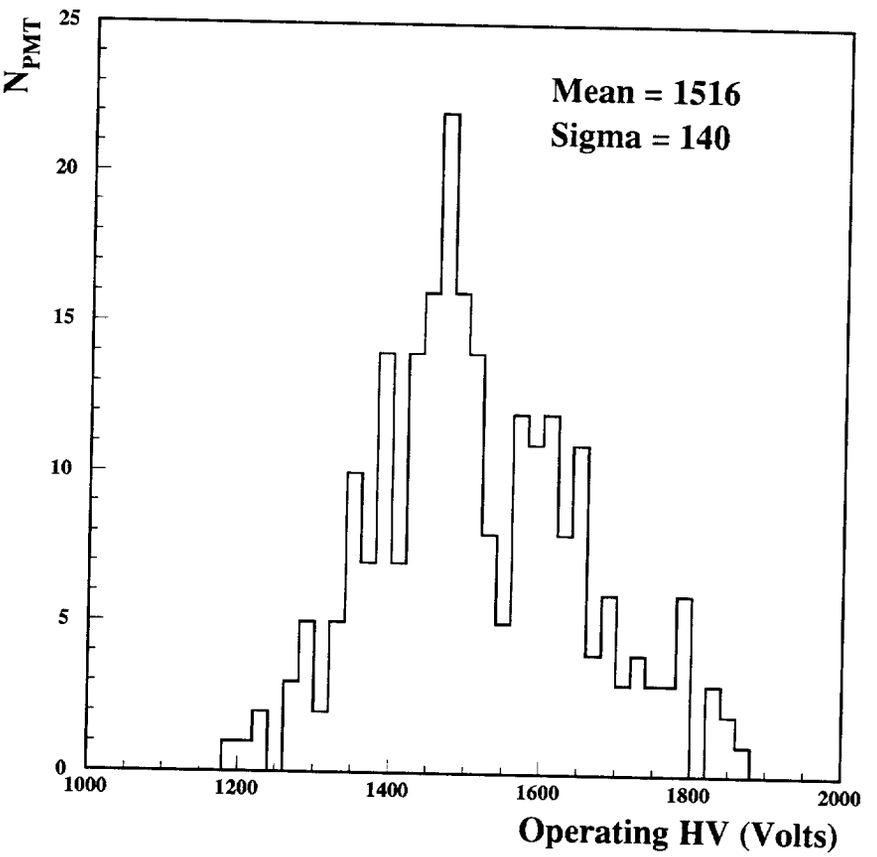


Fig. 6. Operating voltage distribution for PMT pulses corresponding to a gain of 30 $mV/phe$ on 50 $Ohm$.

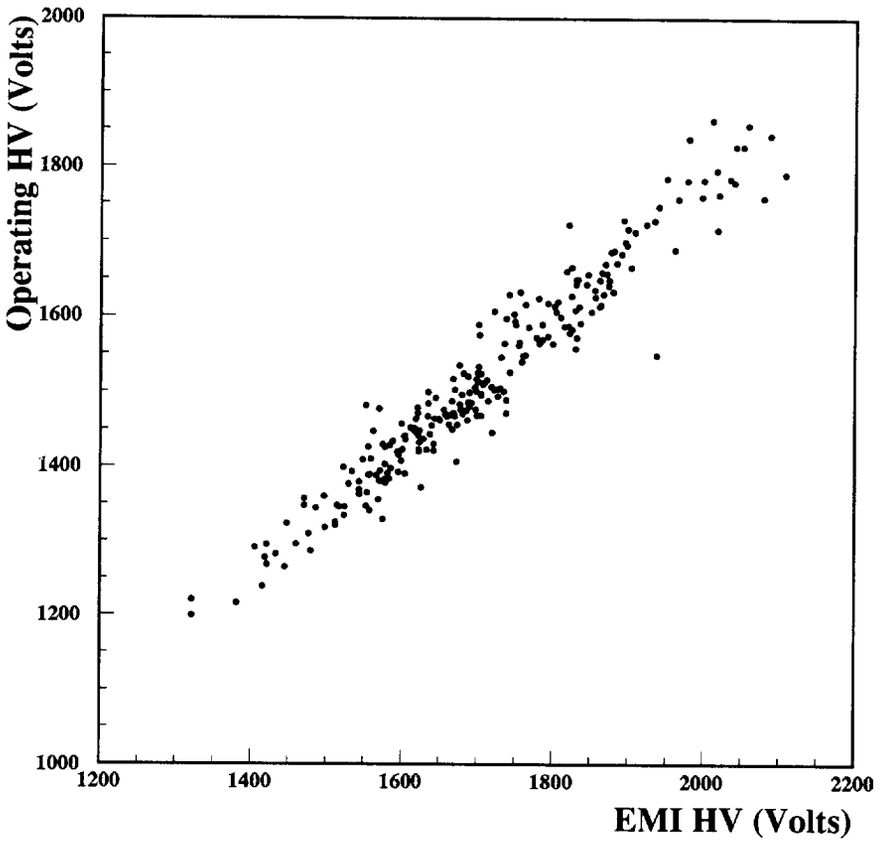


Fig. 7. The comparison between the operating voltages for PMT pulses of 30 $mV/phe$ and EMI voltages for an amplification of 3 $10^7$. (The EMI divider is different from the one we are using).

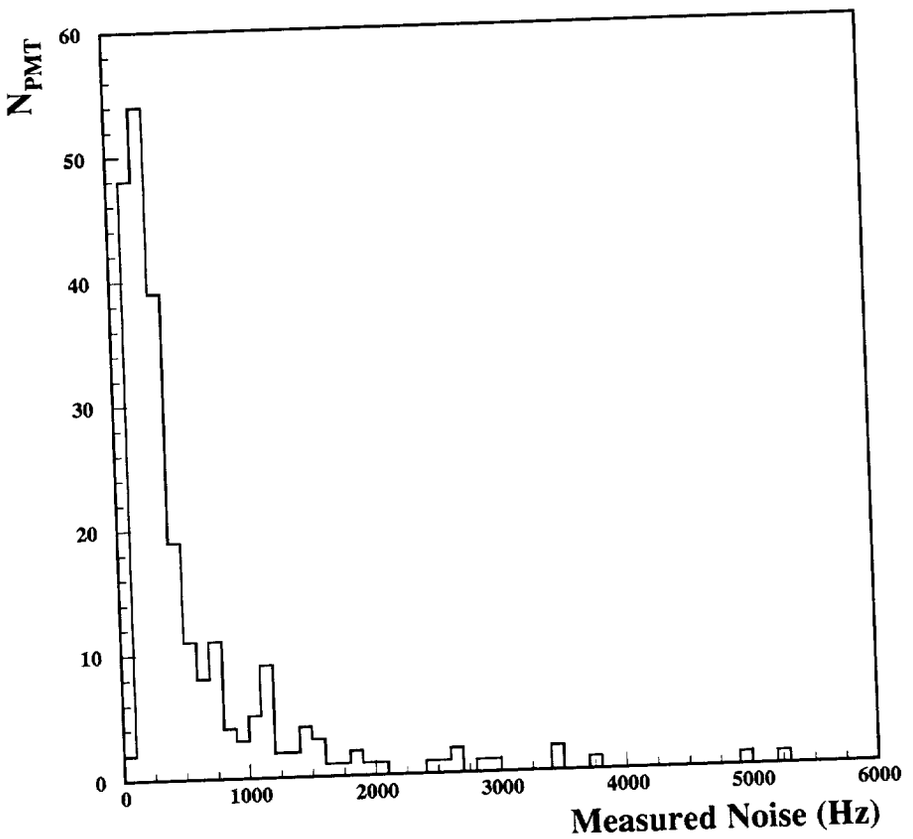


Fig. 8. The dark noise rate distribution; $\approx 12\ h$ since $HV$ turn-on; 30 $mV$ discriminator thresholds; PMT operating voltages.

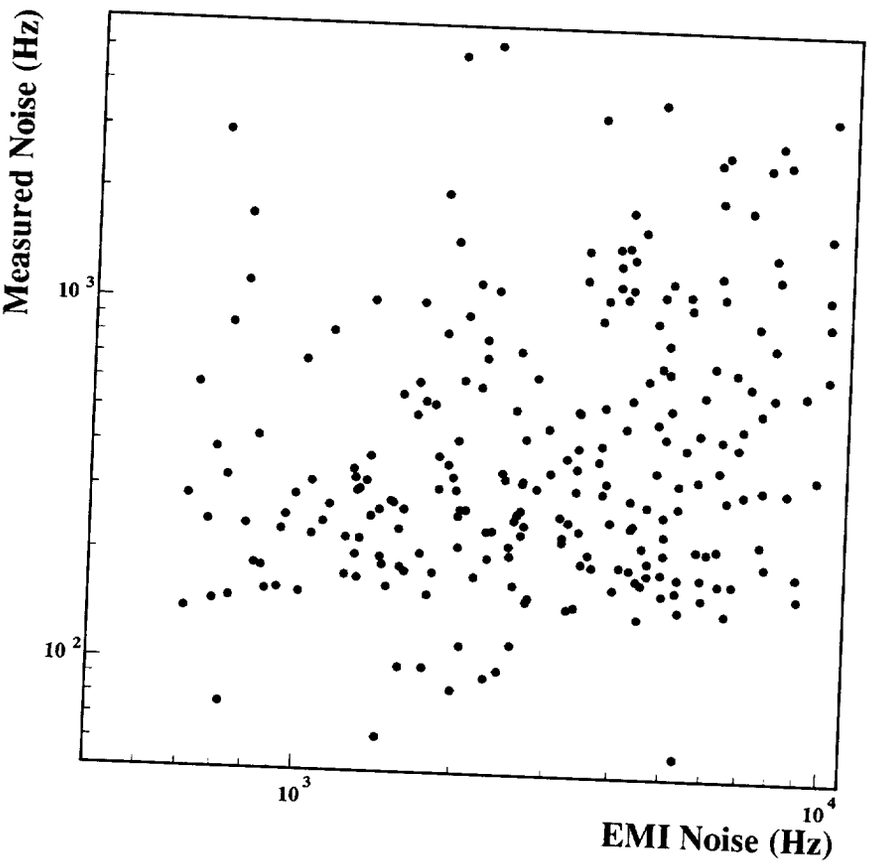


Fig. 9. The comparison of the dark noise rates with the ones measured by EMI.

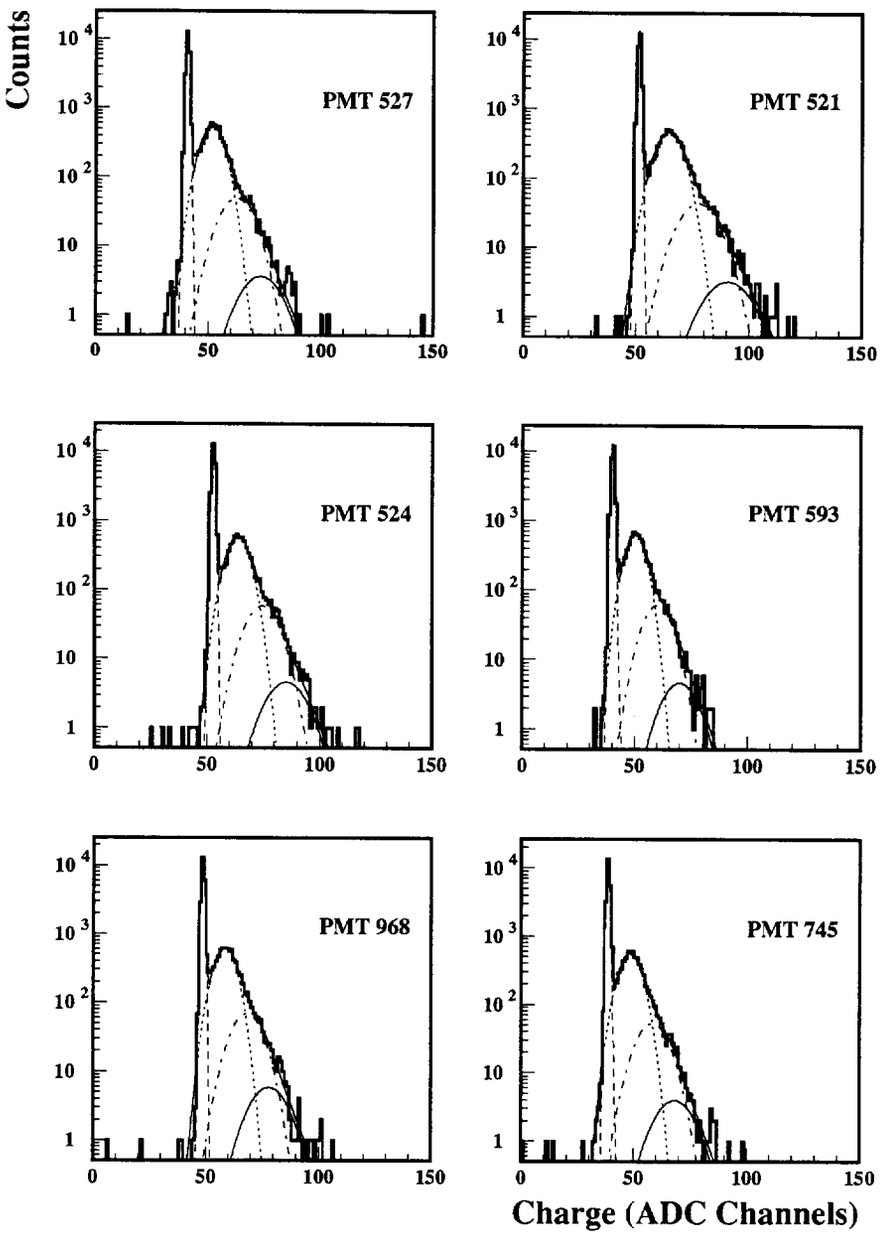


Fig. 10. ADC spectra at the 1-*phe* level; the fits and their 1-, 2-, 3- ...*phes* components are shown.

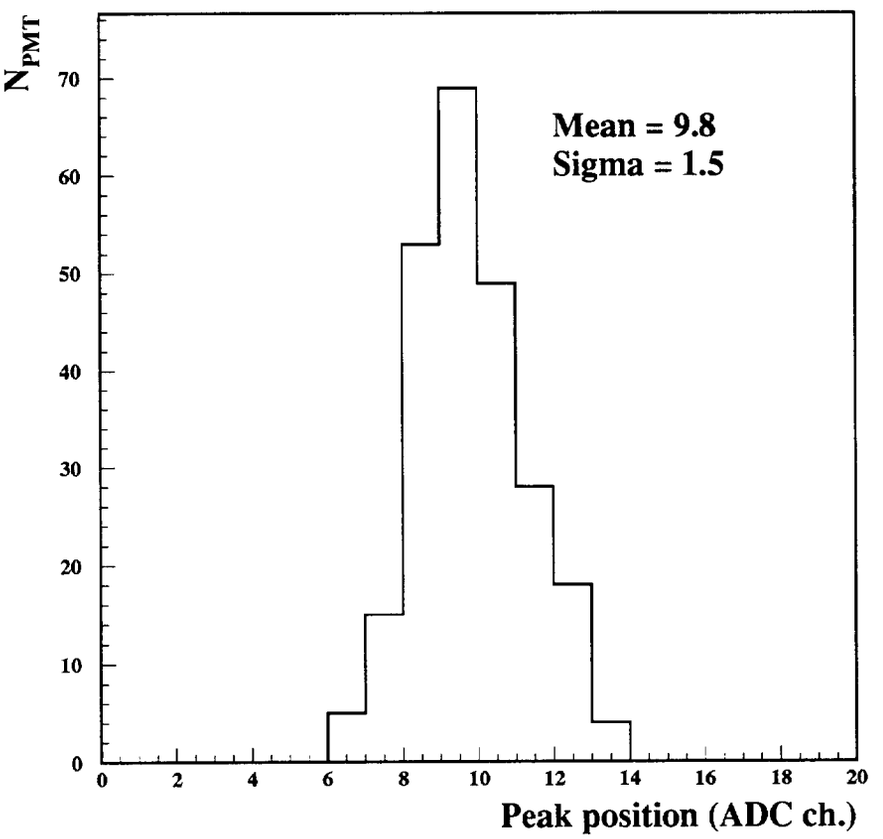


Fig. 11. The distribution of the ADC 1-*phe* spectrum peak positions.

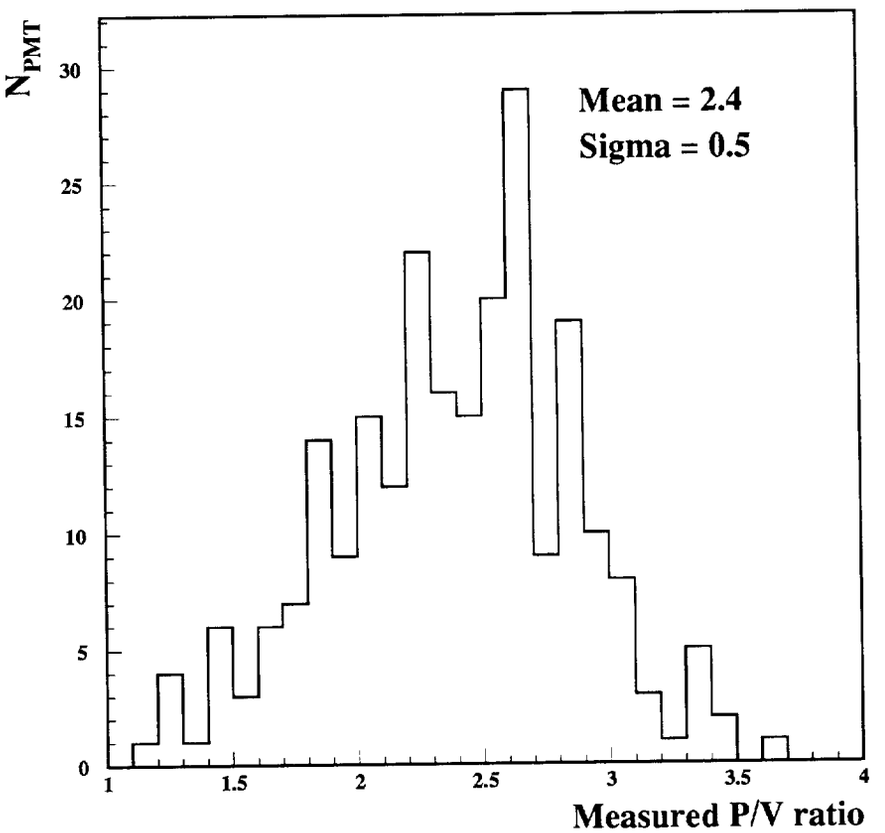


Fig. 12. The distribution of the $P/V$ ratios.

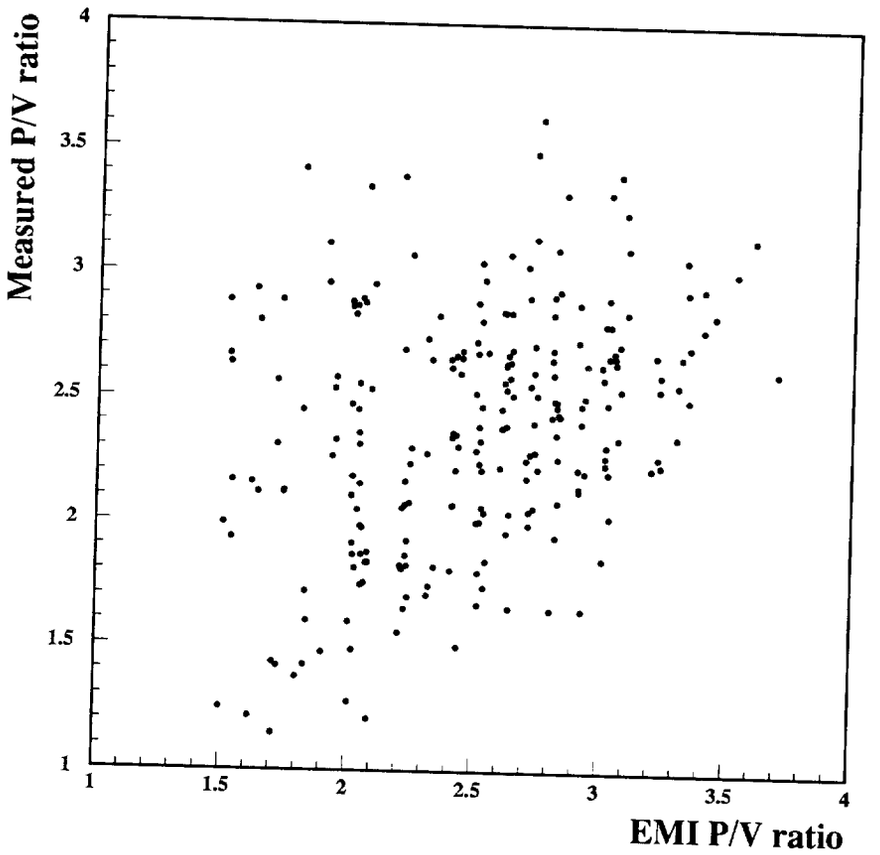


Fig. 13. The comparison of the $P/V$ ratios with the ones measured by EMI.

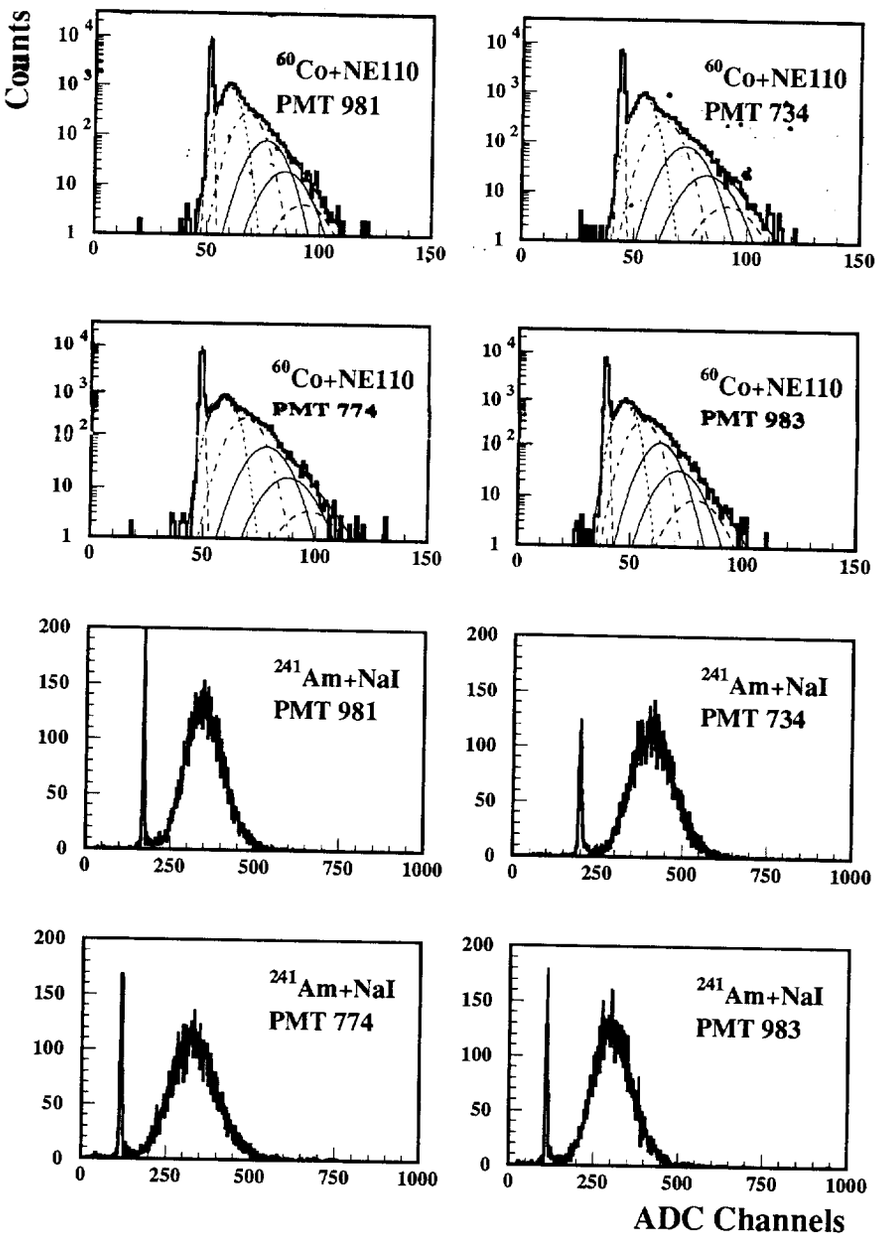


Fig. 14. ADC spectra by the $NE110 + ^{60}Co$ and by the $NaI + ^{241}Am$ light pulsers; the fits to the $NE110$ data are shown.

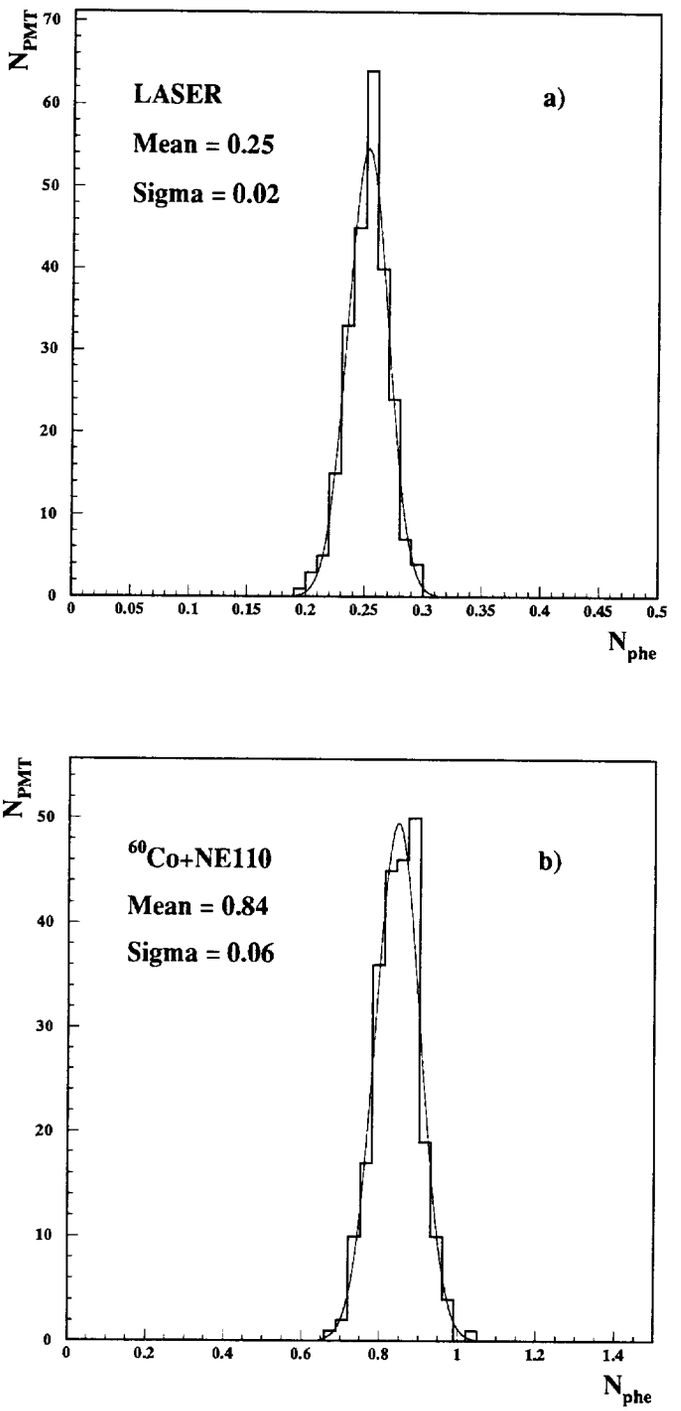


Fig. 15. The PMT relative sensitivity distributions. a) measured by laser; b) measured by $NE110$; gaussian fits are superimposed.

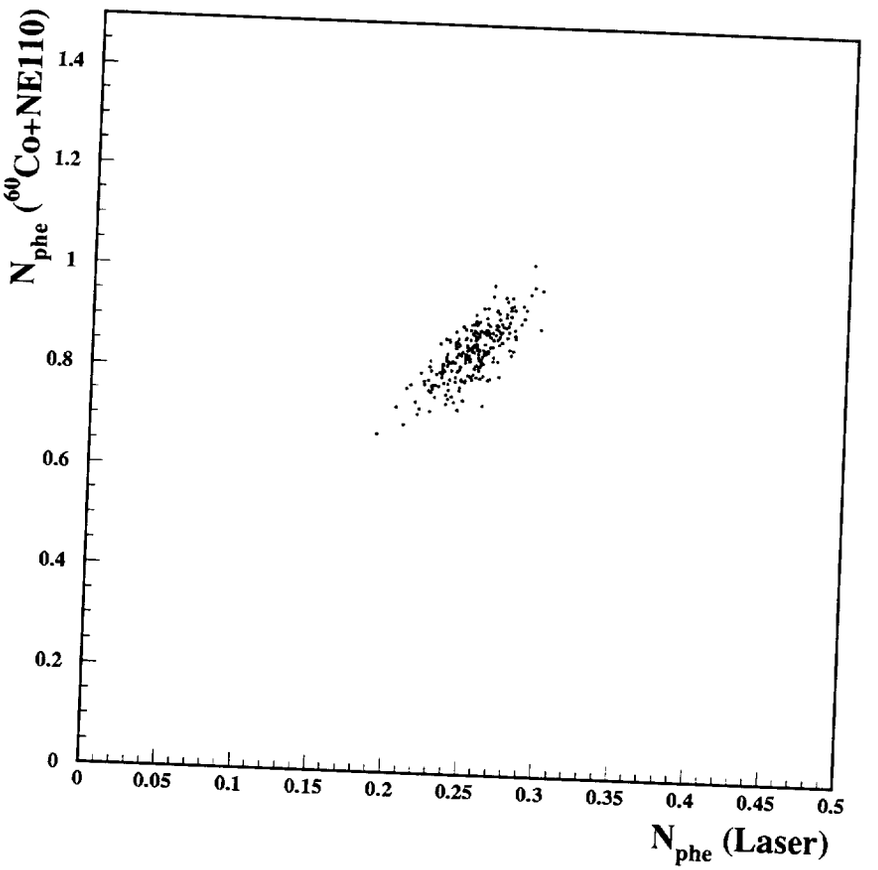


Fig. 16. The relative PMT sensitivity measured by $NE110 + ^{60}Co$ vs. the relative sensitivity measured by laser light.

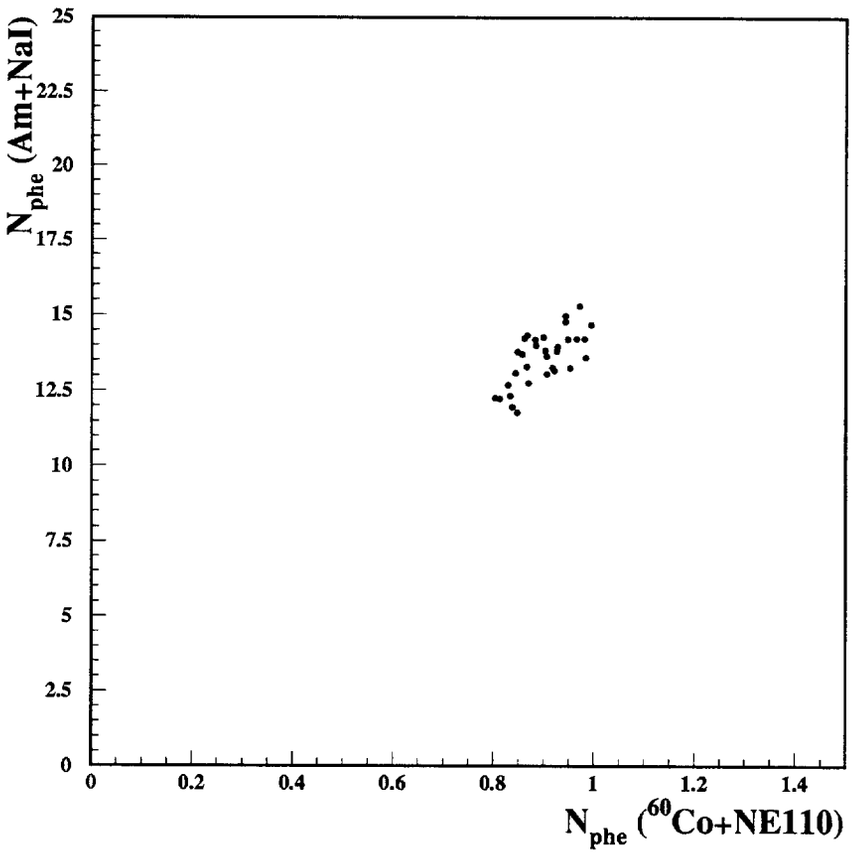


Fig. 17. The relative PMT sensitivity measured by $NE110 + {}^{60}Co$ vs. the relative sensitivity measured by $NaI + {}^{241}Am$.

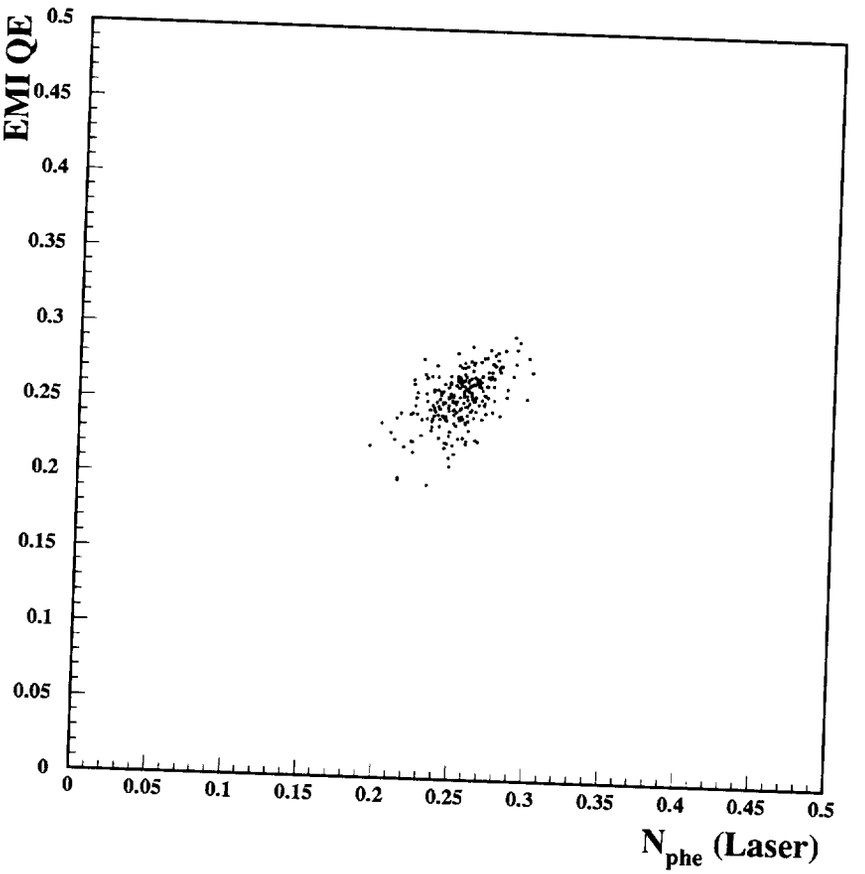


Fig. 18. $QE$ measured by EMI vs. the PMT sensitivity (proportional to $QE \times CE$) measured by laser light.

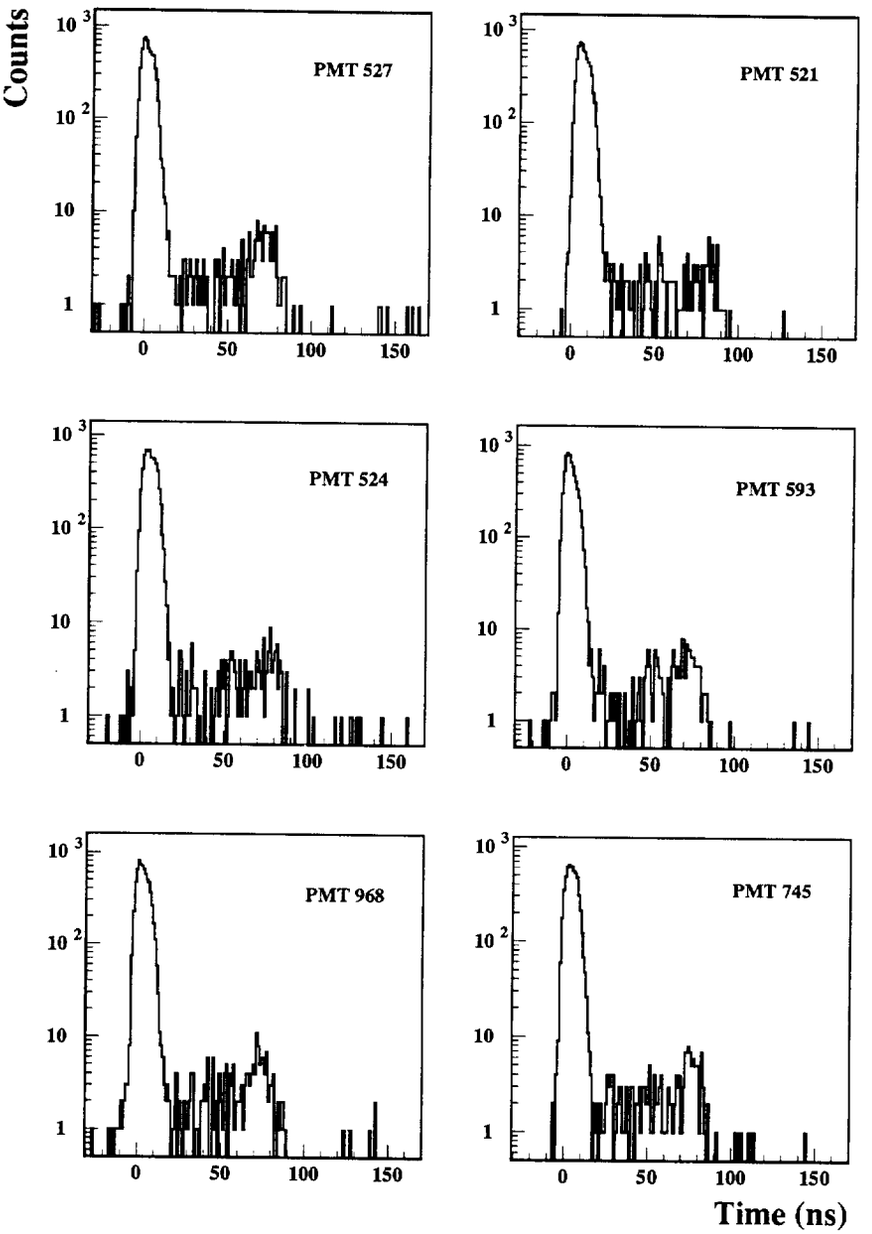


Fig. 19. The TDC spectra at the 1-*phe* level.

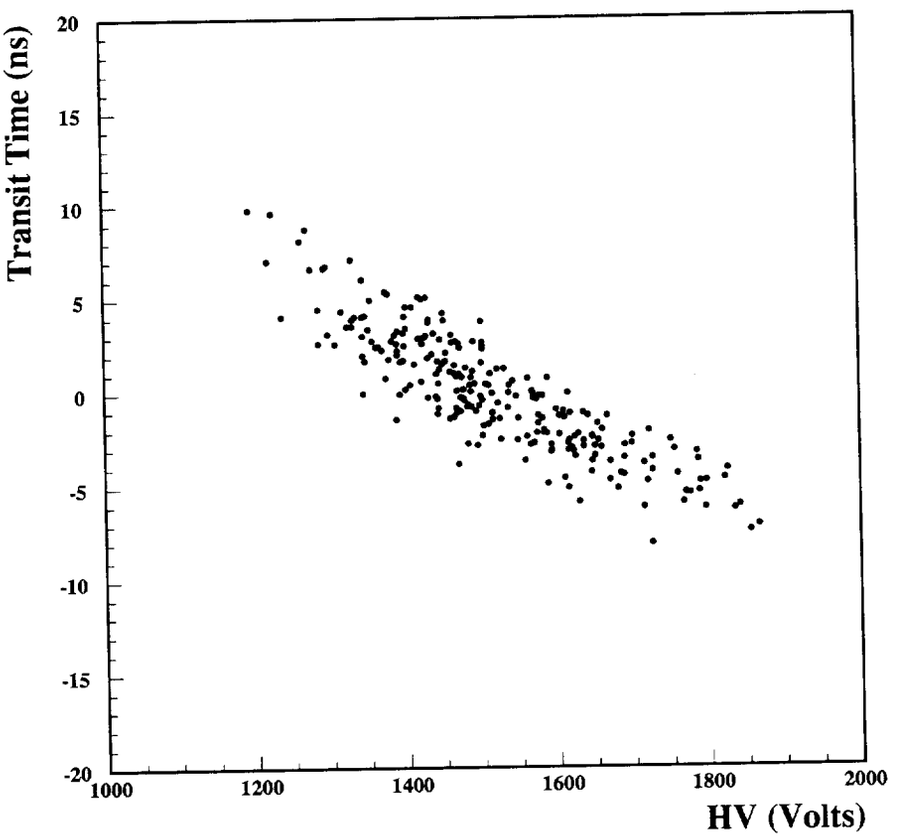


Fig. 20. The relative transit time vs. the PMT operating voltage.

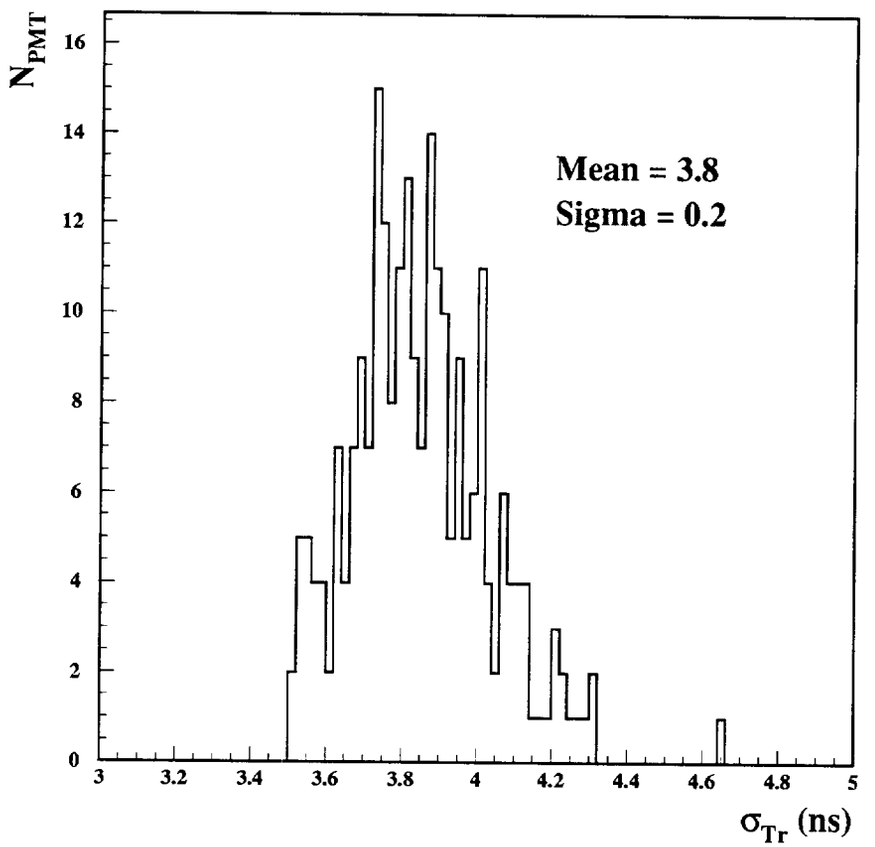


Fig. 21. The distribution of the transit time fluctuations $\sigma_{Tr}$ ; 1-*phe* light level; PMT operating voltages.

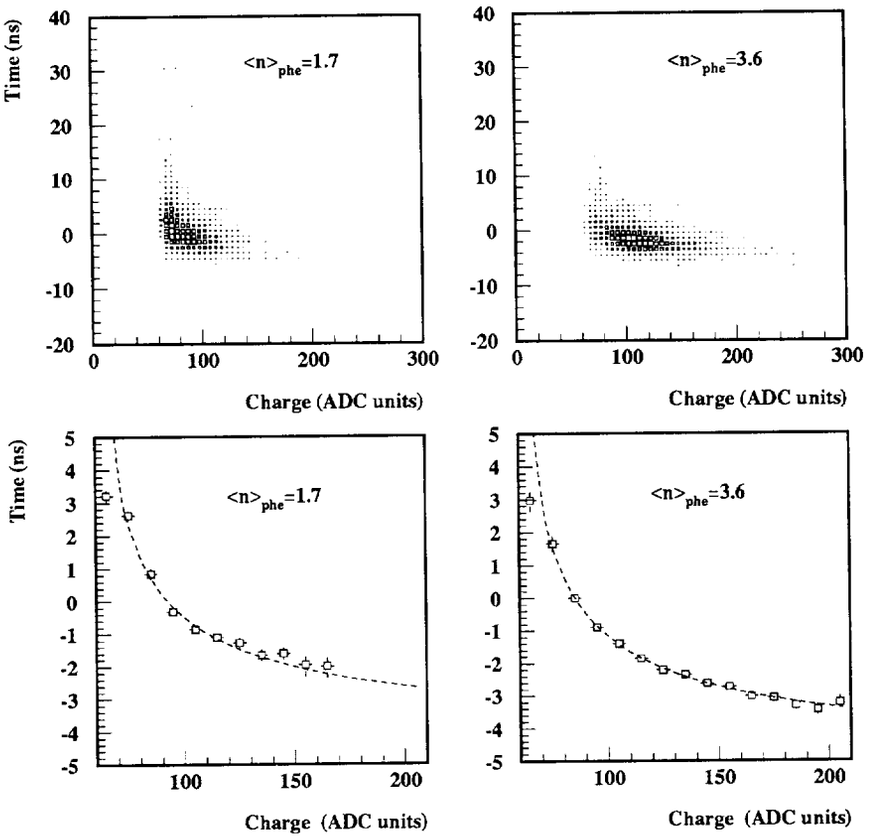


Fig. 22. Slewing-time effects at two different light levels. a) scatter plots; b) average time slewing.

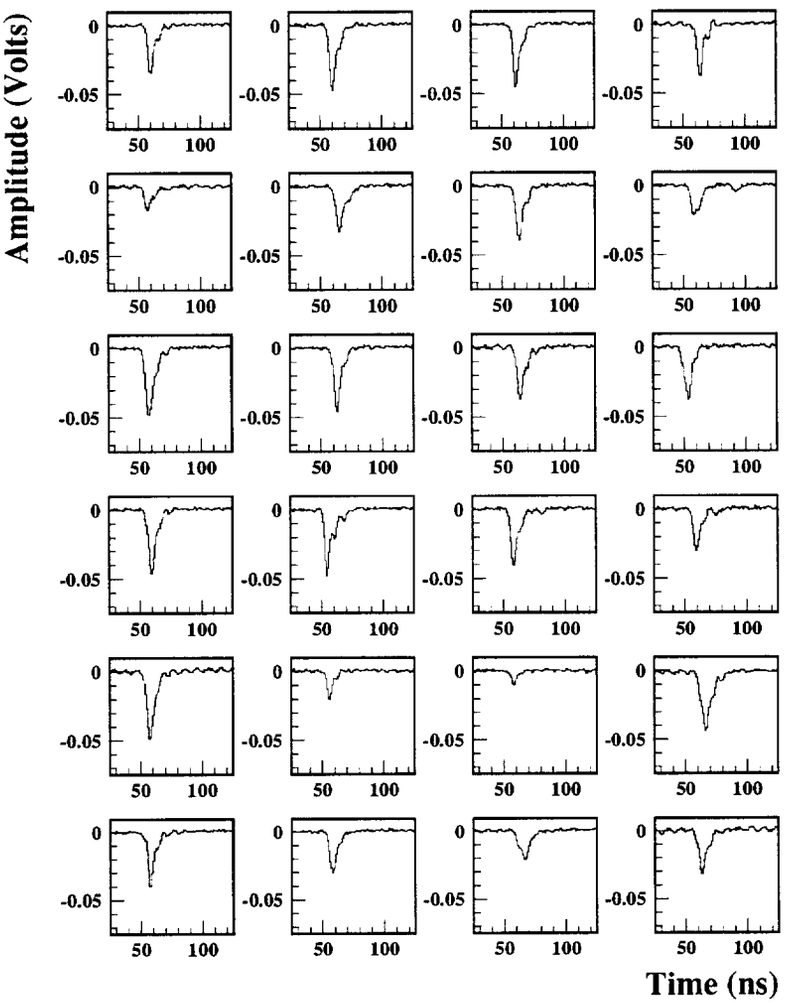


Fig. 23. PMT pulse waveforms at the 1-*phe* light level.